Systematic Approach for Electrically Tuning N-port Antenna System Based on Characteristic Modes

Montaha Bouezzeddine, Werner L. Schroeder

RheinMain University of Applied Sciences, GERMANY
e-mail: {montaha.bouezzeddine|werner.schroeder}@hs-rm.de

***Abstract*—We develop, in this paper, a systematic approach to be applied for matching/tuning N-port symmetric antenna system whose design is based on the characteristic modes of a device. The approach uses conformal mapping techniques and allows us to study the feasibility and possible implementation of a "joint matching" to simultaneously match several radiation modes. The approach helps to conclude about the available modes that could be physically matched and to decide about possibly making some amendments on the antenna design. It renders the tuning range of elements of the tunable matching network. Theoretical derivation is supported by the measured scattering parameters of a MIMO antenna system operating in the range** $[470, 790]$ MHz**.**

I. Introduction

The need for tunable Multiple Input – Multiple Output (MIMO) antennas on small platforms has increased during the last years. Many designs for multi-band and broadband applications have been suggested like [1]–[3]. In the cited papers, authors present designs based on the theory of Characteristic Modes (CMs) and limited to 2-port MIMO antenna system. In case couplers can be grouped into sets such that each set of couplers excites a superposition of current distributions which is orthogonal to all other superpositions [4], each set of couplers can be matched individually.

For a general N-port antenna, however, the task of matching also comprises decoupling of ports. This task becomes complex for wideband applications and $N > 2$. Solutions based on symmetries and CMs as in [5]–[7] provide a high isolation between the Radiation Modes (RMs) of the antenna system [8]. Authors in [6] apply a selective excitation with a distinct set of couplers for each of the three CMs. This solution facilitates the matching problem, but the number of couplers exceeds significantly the number of RMs. For an antenna system with large N, using the same set of couplers to excite several modes may be unavoidable, but creates many challenges especially in wideband applications. The most challenging aspect of designs with common excitation of CMs is the simultaneous matching of several modes. This problem was raised, without being solved, in [5]. In [7], we report about the first wideband design featuring simultaneous matching of multiple RMs which are excited by means of a common set of couplers. Simultaneous matching, directly at the coupler ports, is required to avoid a large mismatch at the ports of the Decoupling Network (DN). Matching between the couplers and the DN is necessary to shorten the resonant current path and diminish the overall antenna system losses. Otherwise, a degradation of the modal efficiencies and of isolation between the modal ports may result. In this paper, we derive a design procedure for tunable matching networks which are suitable for simultaneous matching of several RMs directly at the coupler ports.

II. Radiation modes and Modal Reflectances

Consider an N-port antenna system characterized by its scattering matrix $\mathbf{S}^{\mathrm{A}}$. The modal reflectances are obtained as elements of the diagonal matrix

$$\mathbf{\Gamma} = \mathbf{diag}(\Gamma_1, \Gamma_2, ...\Gamma_{\mathrm{N}}) = \mathbf{V}^{\top}\mathbf{S}^{\mathrm{A}}\mathbf{V} \tag{1}$$

where $\mathbf{V}$ is a unitary matrix, its columns are the RMs of the multi-port antenna system [8]. We consider here the special, but practically most relevant case, where each RM has a one-to-one correspondence to a set of *characteristic modes* of the device, the sets being defined by mutually exclusive symmetry properties. In this case, $\mathbf{V}$ is defined by symmetry, therefore it is frequency independent and real, i.e. it satisfies the condition

$$\mathbf{V}^{\top}\mathbf{V} = \mathbf{I}_N \tag{2}$$

where $\mathbf{I}_N$ denotes the identity matrix of dimension $N \times N$. The modal decomposition after (1) can be realized by a DN, with the scattering matrix [9]

$$\mathbf{S}_{\mathrm{DN}} = \begin{pmatrix} 0 & \mathbf{V} \\ \mathbf{V}^{\top} & 0 \end{pmatrix}, \tag{3}$$

directly placed at the coupler ports as indicated in Fig. 1a. A subsequent $2N$-port Matching Network (MN) with scattering matrix $\mathbf{S}_{\mathrm{M}}$ is also shown in Fig. 1a. In this arrangement, the MN can be decomposed into N *distinct* 2-port matching networks to individually match each mode. Under the condition expressed by (2), the application of the identical MN at all coupler ports is equivalent to the application of the same MN to all RMs, i.e. the operations "matching" and "decomposition" can commute if we ignore losses. This observation is relevant for the design, because it tells that $\mathbf{S}_{\mathrm{M}}$ is to be chosen so as to match modes, although it is to be placed directly at the coupler ports as shown in Fig. 1b. In [7], we illustrated the advantage of the sequence shown in Fig. 1b with respect to modal efficiencies.

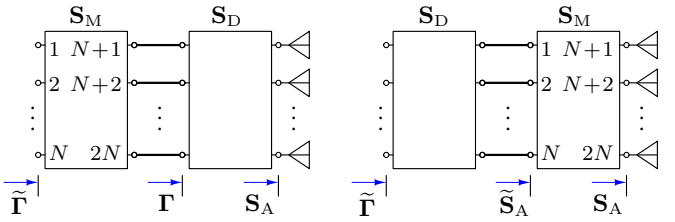

(a) (a)

Fig. 1. Modal decomposition and matching commute if $\mathbf{S}_\mathrm{D}$ satisfies (3) and $\mathbf{S}_\mathrm{M}$ conforms to (4).

As a proof of the equivalence of Figs. 1a,b, we compare the scattering matrices at the outer feed ports of the MN block. For both sketches, the $2N$-port MN actually decomposes into N separate 2-port MNs. Its scattering matrix is of the simple block-diagonal form

$$\begin{pmatrix} \mathbf{S}_{\mathrm{M}11} & \mathbf{S}_{\mathrm{M}12} \\ \mathbf{S}_{\mathrm{M}21} & \mathbf{S}_{\mathrm{M}22} \end{pmatrix} = \begin{pmatrix} s_{\mathrm{M}11}\mathbf{I}_N & s_{\mathrm{M}12}\mathbf{I}_N \\ s_{\mathrm{M}21}\mathbf{I}_N & s_{\mathrm{M}22}\mathbf{I}_N \end{pmatrix}. \tag{4}$$

For the arrangement shown in Fig. 1a, the scattering matrix with respect to the feed ports $1,\ldots,N$ is

$$\mathbf{S}_\mathrm{P}^{(a)} = \widetilde{\mathbf{\Gamma}} = s_{\mathrm{M}11}\mathbf{I} + s_{\mathrm{M}21}^2\mathbf{\Gamma}(\mathbf{I}_{2N} - s_{\mathrm{M}22}\mathbf{\Gamma})^{-1}, \tag{5}$$

and for the arrangement after Fig. 1b, it becomes

$$\begin{aligned} \mathbf{S}_\mathrm{P}^{(b)} &= \mathbf{V}^\top\Big(s_{\mathrm{M}11}\mathbf{I} + s_{\mathrm{M}21}^2\mathbf{V}\mathbf{\Gamma}\mathbf{V}^\top(\mathbf{I}_{2N} - s_{\mathrm{M}22}\mathbf{V}\mathbf{\Gamma}\mathbf{V}^\top)^{-1}\Big)\mathbf{V} \\ &= s_{\mathrm{M}11}\mathbf{I} + s_{\mathrm{M}21}^2\mathbf{\Gamma}\Big(\mathbf{V}^\top(\mathbf{I}_{2N} - s_{\mathrm{M}22}\mathbf{V}\mathbf{\Gamma}\mathbf{V}^\top)\mathbf{V}\Big)^{-1} \qquad (6) \\ &= s_{\mathrm{M}11}\mathbf{I} + s_{\mathrm{M}21}^2\mathbf{\Gamma}(\mathbf{I}_{2N} - s_{\mathrm{M}22}\mathbf{\Gamma})^{-1} = \widetilde{\mathbf{\Gamma}}. \qquad (7) \end{aligned}$$

Hence we can place the MN between the antenna system and the DN.

III. Procedure for the Design of a Simultaneous Tunable Matching Network of an N-port Antenna System

In this section, we develop the procedure to match N-RMs sharing the same Tunable Matching Network (TMN). Limitations on the number of modes and the frequency interval over which the match is realized are investigated. The steps are summarized in the following points:

(a) Check of feasibility to match all modes to a specified minimum return loss using a simple conformal mapping technique. Design changes are necessary if not and the procedure must be restarted.
(b) Determination of the frequency dependent scattering parameters of a 2-port MN which minimizes Root Mean Square (RMS) magnitude of the reflection coefficient over all RMs.
(c) Determination of topology of a low complexity 2-port MN by inspection of the region to be covered in the Smith-Chart.
(d) Determination of the required parameter range of tunable elements therein from (b) for the topology after (c).
(e) A hardware-in-the-loop optimization to generate the table of optimum tuning states as applied to each sub-band within the target frequency range.

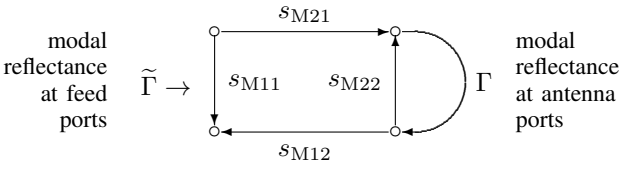

Fig. 2. Signal flow graph with symbols used for discussion of the lossless, reciprocal 2-port matching networks.

A. Feasibility check

The application of *identical* 2-port networks to all modes is of course conditional on the feasibility of simultaneously transforming the original modal reflectances $\Gamma_1(f),\ldots,\Gamma_N(f)$ into a prescribed return loss circle, at any fixed frequency f within the operating frequency range. Since we consider an electrically tunable MN and due to the fact that instantaneous bandwidth is only a fraction of the total operating frequency range, it is sufficient to consider one frequency point at a time. Let $D(f)$ denote a disk in the Smith-Chart which contains $\Gamma_1(f),\ldots,\Gamma_N(f)$. We are then concerned with the question what radius this disk may have to be completely mapped into the prescribed return loss circle by means of a 2-port MN.

For initial design considerations, we consider a lossless and reciprocal 2-port MN (Fig. 2). The scattering parameters of such MN can be expressed in terms of only 3 real parameters $r \in [0,1]$ and $\phi_1, \phi_2 \in [0, 2\pi]$ as

$$\begin{aligned} s_{\mathrm{M}11} &= r\,\mathrm{e}^{\mathrm{j}\,\phi_1}, \quad s_{\mathrm{M}22} = r\,\mathrm{e}^{\mathrm{j}\,\phi_2}, \\ s_{\mathrm{M}12} &= s_{\mathrm{M}21} = \mathrm{j}(1-r^2)\,\mathrm{e}^{\mathrm{j}\,\frac{\phi_1+\phi_2}{2}} \end{aligned} \tag{8}$$

A reflectance Γ, seen at port 2, is mapped to input reflectance $\widetilde{\Gamma}$ according to

$$\widetilde{\Gamma} = r\,\mathrm{e}^{\mathrm{j}\,\phi_1} - \frac{(1-r^2)\,\mathrm{e}^{\mathrm{j}(\phi_1+\phi_2)}\,\Gamma}{1 - r\,\mathrm{e}^{\mathrm{j}\,\phi_2}\,\Gamma}. \tag{9}$$

By introducing a complex mapping $F(z)$ as

$$F(z) := r - \frac{(1-r^2)z}{1-rz} = \frac{r-z}{1-rz} = \frac{1}{r}\left(1 + \frac{\frac{1}{r}-r}{z-\frac{1}{r}}\right), \tag{10}$$

we may rewrite (9) in the form

$$\widetilde{\Gamma} = \mathrm{e}^{\mathrm{j}\,\phi_1}\,F(\Gamma\,\mathrm{e}^{\mathrm{j}\,\phi_2}) \tag{11}$$

and, noting that $F(z)$ is its own inverse

$$\Gamma\,\mathrm{e}^{\mathrm{j}\,\phi_2} = F(\widetilde{\Gamma}\,\mathrm{e}^{-\mathrm{j}\,\phi_1}). \tag{12}$$

Since $F(z)$ is a Möbius-transform, it maps generalized circles to generalized circles in the Smith-Chart. To obtain a disk D which is mapped to the disk of radius ρ (corresponding to prescribed magnitude of reflection coefficient) about the origin, we only need to look at the image of the circumscribing circle $\widetilde{\Gamma}(\psi) = \rho\,\mathrm{e}^{\mathrm{j}(\phi_1+\psi)}$ with ψ running through the interval $[0, 2\pi]$ under (12), i.e. at

$$\Gamma(\psi)\,\mathrm{e}^{\mathrm{j}\,\phi_2} = F(\rho\,\mathrm{e}^{\mathrm{j}\,\psi}) \tag{13}$$

The left hand side gives the circumscribing circle of the disk D. Its diameter and the distance of its center from the origin

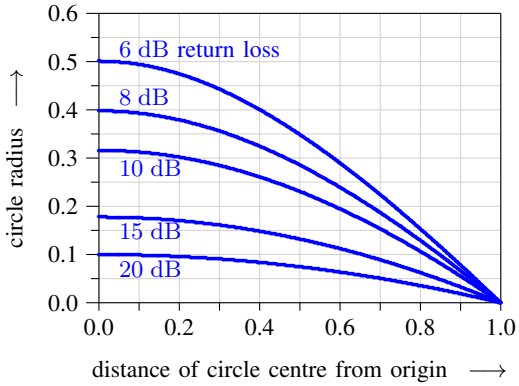

Fig. 3. Radius of matchable disk of distance between its center and the origin of the SMITH-Chart for different return loss requirements.

can be obtained as the difference and mean, respectively, of maximum and minimum of the magnitude of $\Gamma(\psi)$, i.e. from $\max_{\psi} \left|F(\rho\,\mathrm{e}^{\,\mathrm{j}\,\psi})\right|$ and $\min_{\psi} \left|F(\rho\,\mathrm{e}^{\,\mathrm{j}\,\psi})\right|$. From the outermost right form of $F(z)$ in (10), it is easily seen that the maximum and minimum are attained for $\psi = \pi$ and $\psi = 0$, respectively. The values are

$$\max_{\psi} \left|F(\rho\,\mathrm{e}^{\,\mathrm{j}\,\psi})\right| = \frac{r+\rho}{1+r\rho}, \tag{14}$$

$$\min_{\psi} \left|F(\rho\,\mathrm{e}^{\,\mathrm{j}\,\psi})\right| = \frac{r-\rho}{1-r\rho}. \tag{15}$$

The center of the disk D is therefore at distance

$$C(\rho, r) = \frac{1}{2}\left(\frac{r+\rho}{1+r\rho} + \frac{r-\rho}{1-r\rho}\right) = \frac{r(1-\rho^2)}{1-^2\,\rho^2} \tag{16}$$

from the origin of the SMITH-Chart and its radius is

$$R(\rho, r) = \frac{1}{2}\left(\frac{r+\rho}{1+r\rho} - \frac{r-\rho}{1-r\rho}\right) = \frac{\rho(1-r^2)}{1-r^2\rho^2}. \tag{17}$$

The pair of equations (16) and (17) establishes an implicit relation between C and R which reflects a general limitation on the simultaneous matching capability of a lossless reciprocal 2-port. The parameter r can be eliminated by solving (16) for r and substituting into (17). The relation between C and the radius R is then given by

$$-R^2 + C^2 + R\left(\frac{1}{\rho} + \rho\right) - 1 = 0 \tag{18}$$

which defines the equation of an hyperbola. Fig. 3 shows the variation of the radius of the circle R over C, for different return loss requirements. As we see, the circle which encloses the region which maps into the circle of radius ρ about the origin gets smaller as its center gets farther away from the origin of the SMITH-Chart. It becomes a single point, $R = 0$, for loads located at the boundaries of the SMITH-Chart. Obviously, for a fixed distance from the origin, the radius R decreases as the required return loss tends to higher values.

Fig. 4 shows an example for the mapping (12). To be simultaneously matched (at given frequency) into the 10 dB return loss circle (blue), all modal reflectances must be contained in a disk whose radius is R (red) if its center is located on a

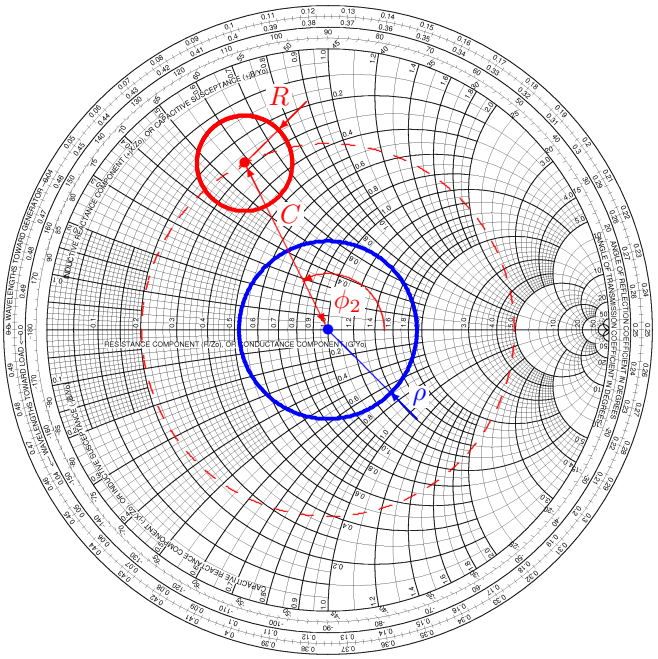

Fig. 4. Example for the image of the 10 dB return loss circle (blue) under the mapping (12) ($C = 0.66246$, $R = 0.16959$).

circle of radius C (dashed). It is a matter of antenna design itself whether this requirement is met. If it is met, we can proceed to the actual design of the 2-port MN.

B. *Specification of* $\mathbf{S}_{\mathrm{M}}$

The frequency dependent scattering parameters of the 2-port matching circuits (Fig. 2) can be derived from the criterion that the RMS of the modal reflectances presented to the DN, i.e. the quantity

$$\left|\widetilde{\Gamma}_{\mathrm{RMS}}(f)\right|^2 := \frac{1}{N}\sum_{n=1}^{N}\left|\widetilde{\Gamma}_n(f)\right|^2 = \frac{1}{N}\sum_{n=1}^{N} F\big(\Gamma_n(f)\,\mathrm{e}^{\,\mathrm{j}\,\phi_2(f)}\big), \tag{19}$$

is minimized. This criterion leads to a relatively simple optimization with respect the two parameters r and ϕ_2 showing up in (8) since the phase ϕ_1 is irrelevant. Starting values for r and ϕ_2 are obtained by setting $r\,\mathrm{e}^{\,-\mathrm{j}\,\phi_2}$ to the approximate center of gravity of the Γ_n. Note that the function F contains the parameter r.

As result of the optimization according to (19), one obtains the frequency dependent scattering matrix of the MN from which the circuit can be synthesized.

C. *Application to a symmetric 4-port antenna system*

Below, the above approach is applied to a 4-port antenna operating in the range $[470, 790]$ MHz and previously described in [7]. The antenna system structure is given in Fig. 5. Following the step described in subsection III.B, we optimize the term $\left|\widetilde{\Gamma}_{\mathrm{RMS}}(f)\right|^2$ for the given example. We plot the modal reflectances of the 4 considered RMs and the trace of the mean of the modal reflectances, denoted by Γ_0 (black trace, green

dots). We add to the graph some of the circles mapped to a 6 dB circle resulting from step described in subsection III.A. To avoid an overlapping of the curves, we plot only 3 circles whose centers are obtained from subsection III.A. The circles are given for some discrete frequencies and do not cover the full range of interest. Fig. 6 shows that physically we cannot match the 4 modes simultaneously, especially at the lower frequency range. This is due to the mode numbered 4. Note that the center of a circle defined by (16) is close to, but not identical with Γ_0. Simultaneous matching is feasible for 3 modes as shown in Fig. 7.

In conclusion the approach allows to determine and select those RMs which can be matched to the desired return loss. For our example, we select 3 modes out of 4. To provide the fourth missing antenna, a monopole is mounted at top of the box. By symmetry, the monopole is decoupled from the modes excited with the couplers and therefore not discussed in the rest of this paper.

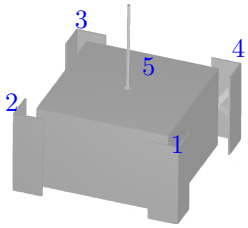

Fig. 5. Simulation model of the 4-port antenna using 4 couplers for excitation of chassis modes [7].

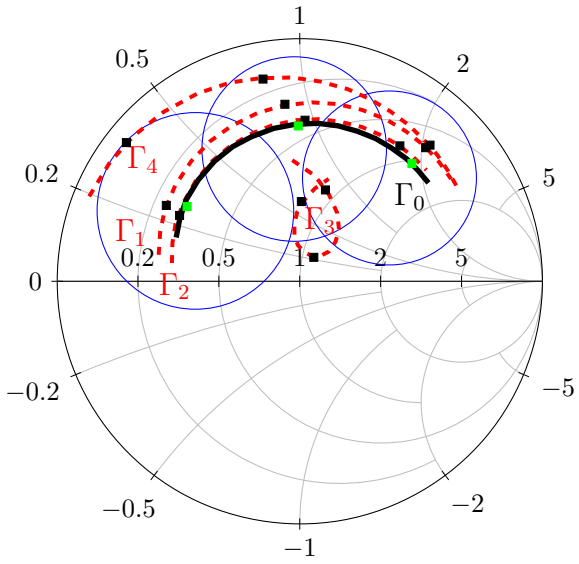

Fig. 6. Modal reflectances of 4 radiation modes (dashed red line), the trace of Γ_0 (solid black line) and mapped 6 dB circles at $\{510, 670, 750\}$ MHz. Markers correspond to these frequencies.

D. Topology of 2-port Matching Network Topology

Contrary to [10], we do not make an a-priori choice of MN topology. The topology is rather determined from the locus of

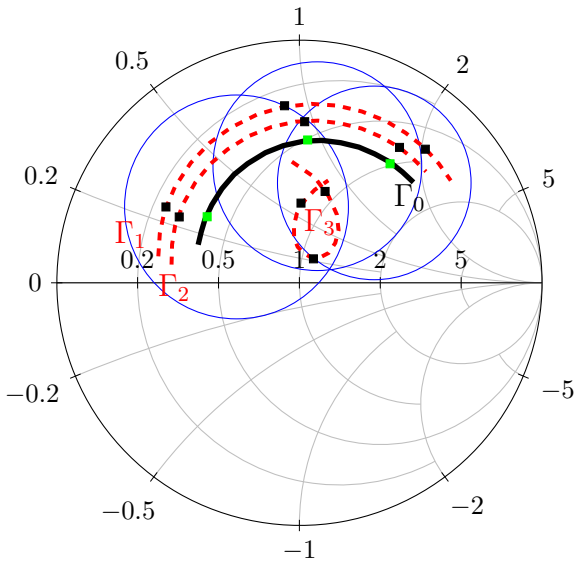

Fig. 7. Modal reflectances of 3 radiation modes (dashed red line), the trace of Γ_0 (solid black) and mapped 6 dB circles at $\{510, 670, 750\}$ MHz. Markers correspond to these frequencies.

average modal reflectance in the SMITH-Chart. Since for the present example all modal reflectance traces are situated in the upper half of the SMITH-Chart, the topology of choice is an L-topology containing a shunt Digitally Tunable Capacitor (DTC) (at port 2) and a series DTC (at port 1). This topology allows, in principle, to match any impedance outside the region enclosed by the red circle in Fig. 8b to match to at least 6 dB return loss. Fig. 8a shows the printed circuit board (PCB) of the MN. For cases where the trajectories of modal reflectances in the SMITH-Chart are longer, switches between MNs may be needed.

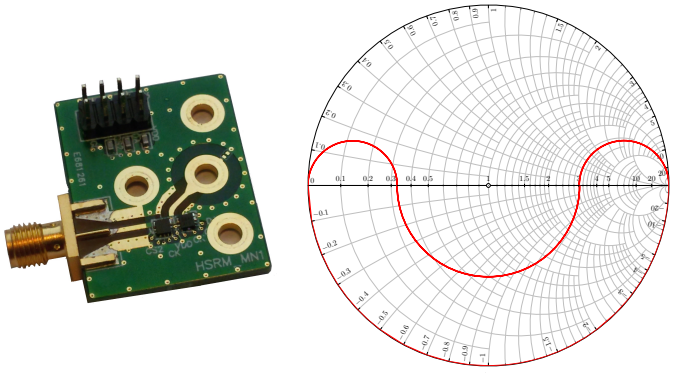

(a) (b)

Fig. 8. (a) The PCB of the tunable matching network of L-type topology made out of 2 DTCs and (b) the forbidden region inside the red contour.

E. Range of Tunable Elements

The optimum s-parameters of the two-port TMN are concluded from the optimization described in subsection III.B. They simultaneously minimize the reflectance of all modes. We can easily determine the required tuning range of the

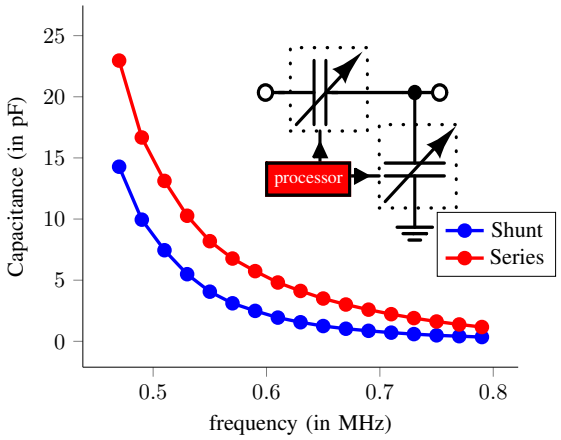

Fig. 9. Required tuning range of the tunable capacitors of the given topology as obtained from the trade-off optimization of the 3 radiation modes.

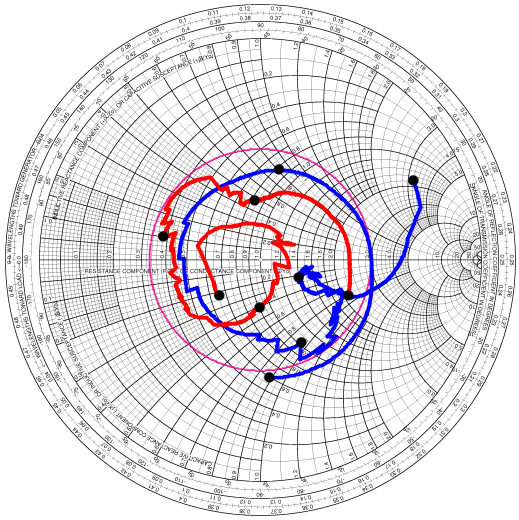

markers at {470,550,630,710,790} MHz

Fig. 10. Measured reflectance traces over 32 bands of 8 MHz bandwidth with tuning separately applied in each band. Results at 2 modal ports.

element of each branch in the topology selected in the step of previous subsection. From the reported range of each element, we conclude about the possible implementations (fixed or tunable elements). For our example, we plot in Fig. 9 the required range of the 2 capacitors.

F. Hardware-in-the-loop optimization

The determination of the range is sufficient for the tunable elements choice. The actual values required for the tunable elements for a given frequency (or set of frequencies if different modes are employed at different frequencies) are preferably obtained in form of a table of tuning states by a hardware-in-the-loop (HIL) optimization. This approach allows to account also for manufacturing inaccuracy and parameter deviations of any element. Fig. 10 shows the measured return loss values obtained for two modes in the range $[470, 790]$ MHz when operating at the same frequency. Only two modes are shown for better visibility, the third mode behaves similarly. A slight degradation of the mode in blue is noticed at the lower range because the DTCs in the present circuit do not meet the required range after Fig. 9. The tuning range of the DTCs is smaller than the theoretically desired range as shown in Fig. 9. We use Serial Peripheral Interface (SPI) controlled devices PE64102 ($[1.88, 14]$ pF) in series configuration and PE64904 ($[1.12, 5.18]$ pF) for the shunt element.

IV. Conclusion

A general procedure for simultaneous matching of RMs of a symmetric N-port antenna has been presented. Using conformal mapping technique, the selection of the modes is concluded from the possibility of simultaneously matching the radiation modes. The properties of the conformal mapping which is realized by a lossless 2-port matching network lead to a criterion for selecting those radiation modes which can be simultaneously matched to the desired level of return loss. The topology of the tunable matching network and the tuning range of the elements are determined consequently. The theoretical results are supported by measurement results for a 4-port antenna system.

Acknowledgment / legal notice: Das diesem Bericht zugrundeliegende Vorhaben wurde mit Mitteln des Bundesministeriums für Bildung und Forschung unter dem Förderkennzeichen 16BU1211 gefördert. Die Verantwortung fur den Inhalt liegt beim Autor.

References

[1] Z. H. Hu, P. Hall, P. Gardner, and Y. Nechayev, "Wide tunable balanced antenna for mobile terminals and its potential for MIMO applications," in *Antennas and Propagation Conference (LAPC), 2011 Loughborough*, Nov 2011, pp. 1–4.

[2] J.-H. Lim, Z.-J. Jin, C.-W. Song, and T.-Y. Yun, "Simultaneous frequency and isolation reconfigurable MIMO PIFA using PIN diodes," *Antennas and Propagation, IEEE Transactions on*, vol. 60, no. 12, pp. 5939–5946, Dec 2012.

[3] Z. Miers, H. Li, and B. K. Lau, "Design of bandwidth-enhanced and multiband MIMO antennas using characteristic modes," *Antennas and Wireless Propagation Letters, IEEE*, vol. 12, pp. 1696–1699, 2013.

[4] A. Krewski, W. Schroeder, and K. Solbach, "MIMO LTE antenna design for laptops based on theory of characteristic modes," in *Antennas and Propagation (EUCAP), 2012 6th European Conference on*, March 2012, pp. 1894–1898.

[5] S. Chaudhury, H. Chaloupka, and A. Ziroff, "Novel MIMO antennas for mobile terminal," in *Microwave Conference, 2008. EuMC 2008. 38th European*, 2008, pp. 1751–1754.

[6] R. Martens, E. Safin, and D. Manteuffel, "Selective excitation of characteristic modes on small terminals," in *Antennas and Propagation (EUCAP), Proceedings of the 5th European Conference on*, April 2011, pp. 2492–2496.

[7] M. Bouezzeddine and W. L. Schroeder, "'Wideband decoupling and tunable matching networks for multi-port antennas," in *The 8th European Conference on Antennas and Propagation (EuCAP 2015)*, Lisbon, Portugal, Apr. 2015, pp. 3169–3173.

[8] S. Stein, "On cross coupling in multiple-beam antennas," *Antennas and Propagation, IRE Transactions on*, vol. 10, no. 5, pp. 548–557, September 1962.

[9] W. Kahn, "Active reflection coefficient and element efficiency in arbitrary antenna arrays," *Antennas and Propagation, IEEE Transactions on*, vol. 17, no. 5, pp. 653–654, Sep 1969.

[10] M. Thompson and J. Fidler, "Determination of the impedance matching domain of impedance matching networks," *Circuits and Systems I: Regular Papers, IEEE Transactions on*, vol. 51, no. 10, pp. 2098–2106, Oct 2004.